HHS Public Access

Author manuscript

Nat Commun. Author manuscript; available in PMC 2015 October 23.

Published in final edited form as:

Nat Commun. ; 6: 6807. doi:10.1038/ncomms7807.

Direct neuronal glucose uptake heralds activity-dependent increases in cerebral metabolism

Iben Lundgaard[1], **Baoman Li**[1], **Lulu Xie**[1], **Hongyi Kang**, **Simon Sanggaard**, **John Douglas R Haswell**, **Wei Sun**, **Siri Goldman**, **Solomiya Blekot**, **Michael Nielsen**, **Takahiro Takano**, **Rashid Deane**, and **Maiken Nedergaard**

Center for Translational Neuromedicine, University of Rochester, Rochester, NY 14642 USA and Center for Basic and Translational Neuroscience, Faculty of Health and Medical Sciences, University of Copenhagen, DK-2200 Copenhagen N, Denmark

Abstract

Metabolically, the brain is a highly active organ that relies almost exclusively on glucose as its energy source. According to the astrocyte-to-neuron lactate shuttle hypothesis, glucose is taken up by astrocytes and converted to lactate, which is then oxidized by neurons. Here we show, using 2-photon imaging of a near-infrared 2-deoxyglucose analogue (2DG-IR), that glucose is taken up preferentially by neurons in awake behaving mice. Anesthesia suppressed neuronal 2DG-IR uptake and sensory stimulation was associated with a sharp increase in neuronal, but not astrocytic, 2DG-IR uptake. Moreover, hexokinase, which catalyze the first enzymatic steps in glycolysis, was highly enriched in neurons compared with astrocytes, in mouse as well as in human cortex. These observations suggest that brain activity and neuronal glucose metabolism are directly linked, and identifies the neuron as the principal locus of glucose uptake as visualized by functional brain imaging.

Functional brain imaging has, in recent years, revolutionized our understanding of complex neural processing. Positron emission tomography (PET) imaging of glucose analogues takes advantage of the fact that glucose is the major energy substrate that fuels neural activity. Unlike other organs, the brain does not use fatty acid oxidation as a source of energy and is highly dependent on glucose for sustenance (1, 2). However, a point of contention is that functional imaging techniques rely on surrogate markers of neural activity and thus leave questions as to whether a direct relationship exists between neuronal activity and metabolic surrogates. Interpretation of activity-dependent glucose uptake is complex due to competing theories of central nervous system (CNS) glucose metabolism. According to one theory, the astrocyte-to-neuron lactate shuttle hypothesis, energy metabolism is compartmentalized and

---

Corresponding authors: Maiken Nedergaard (Nedergaard@URMC.Rochester.edu) or Iben Lundgaard (Iben_Lundgaard@URMC.Rochester.edu), Division of Glial Disease and Therapeutics, Center for Translational Neuromedicine, University of Rochester, 601 Elmwood Avenue, Rochester, NY 14642.

[1]These authors contributed equally to the work

Author contributions: IL, LX, BL, RD and MN designed and interpreted experiments. IL, LX, BL, RD, HK, SS, JDRH, WS, SG, SB, MH and TT performed experiments and analyzed data. IL, LX, BL, RD and MN wrote the manuscript.

Competing financial interests: The authors declare no competing financial interests.

glycolysis is outsourced to astrocytes (3–8). This model proposes that glucose is primarily taken up by astrocytes located around blood vessels and converted to lactate. In turn, neuronal energy metabolism relies chiefly on import of lactate and the energetically favorable process of mitochondrial lactate oxidation (3–7). A consequence of the astrocyte-to-neuron lactate shuttle hypothesis is that glucose metabolism in activated brain regions only indirectly reflects neuronal metabolism and that functional brain imaging might not provide accurate information concerning neuronal activity. The opposing view is the parsimonious hypothesis - that neurons take up glucose directly from the interstitium and generate ATP from both glycolysis and oxidative metabolism. (9–12). In order to correctly interpret human brain imaging it is therefore of defining importance to discern which population of cells increases glucose uptake during complex neural processing. Here, we have used *in vivo* 2-photon imaging of a near-infrared glucose analogue to assess cellular glucose uptake (13, 14). We report findings that support the parsimonious model by showing that neurons, and not astrocytes, during rest as well as during activity-dependent increases in neural activity, are the primary consumers of glucose. Further experiments used a combination of genomic expression analysis and quantitative immunohistochemistry to evaluate neuronal versus astrocytic expression of hexokinases. Hexokinases catalyze the first step of glycolysis in which glucose is converted to glucose-6-phosphate. All the intermediary products of the glycolytic pathway, including glucose-6-phosphate, are impermeable to the plasma membrane and are, thereby, trapped within the cytosol. Products of glycolysis can first exit the cells after they are metabolized to either pyruvate or lactate, or oxidized to CO_2 and H_2O (15, 16). Accordingly, hexokinase can be regarded as the gatekeeper senzymatic step of glycolysis, since their expression correlates directly with the rate of glucose metabolism across multiple regions, including cortex, hippocampus and retina (17). Our analysis showed that neurons consistently expressed higher level of hexokinases than astrocytes in both mouse and human brain.

Results

Validation of the 2DG-IR glucose probe

A major challenge in assessing neuronal and astrocyte energy metabolism has been the inability to image glucose uptake with cellular resolution *in vivo*. The majority of studies on neuronal versus astrocytic glucose uptake have therefore been limited to cell culture or brain slice models. In the pursuit of improving the analysis of cellular glucose uptake, we assessed a near-infrared 2-deoxyglucose probe (IRDye 800CW 2DG, 2DG-IR). Due to its low energy wavelength absorption this compound is used for imaging of glucose consumption in live animals and can reliably track tumor growth *in vivo* (13, 14). We first compared 2DG-IR uptake to that of ^{14}C-glucose and ^{14}C-2-deoxyglucose (^{14}C-2DG) in both primary neurons and astrocytes *in vitro* (18, 19) (Fig. 1a). The initial analysis showed that cultured neurons exhibited a 4-fold higher rate of glucose itself uptake (^{14}C-glucose) than cultured astrocytes (Fig. 1b). The glucose analogue, ^{14}C-2DG, was also taken up several-fold faster in neuronal than astrocytic cultures (Fig. 1c). Radiolabeled 2DG has been extensively used to study functional activation, since Sokoloff and co-workers discovered that 2DG after phosphorylation to glucose-6-phosphate is trapped in neural cells due to the low expression of glucose-6 phosphatase in brain (20). In particular, [^{18}F]2-fluoro-2-deoxy-D-glucose

(^{18}FDG) has routinely been employed in PET studies to identify activity dependent increases in local metabolic activity in human subjects (21). To obtain cellular resolution of glucose uptake, we next compared the uptake of the near-infrared 2DG glucose analogue (2DG-IR) in cultured neurons and astrocytes to ^{14}C-2DG. Similar to ^{14}C-2DG uptake, neurons exhibited a several fold higher rate of 2DG-IR uptake than astrocytes (Fig. 1c). Substrate competition analysis showed that D-glucose suppressed ^{14}C-2DG and 2DG-IR uptake in a concentration-dependent manner (Fig. 1d). Moreover, cytochalasin B, a nonspecific glucose transport inhibitor, also strongly inhibited the uptake of ^{14}C-glucose, ^{14}C-2DG and 2DG-IR in neuronal and astrocytic cultures (Fig. 1e–f). Collectively, our *in vitro* analysis showed that neurons outcompete astrocytes with regard to uptake of glucose itself, as well as with uptake of radio- and fluorescence-labeled 2DG. Moreover, the similarities of response to substrate inhibition and cytochalasin B inhibition suggest that both ^{14}C-2DG and 2DG-IR uptake is dependent on plasma membrane glucose transporters, as previously documented for ^{14}C-2DG and another fluorescent 2DG analogue, 2-NBDG (22, 23).

In vivo 2-photon imaging of awake mice shows high 2DG-IR uptake in neurons

To compare neuronal vs astrocytic 2DG-IR uptake *in vivo*, we next administered 2DG-IR into the peri-arterial Virchow-Robin space surrounding large penetrating cortical arteries. Using *in vivo* 2-photon excitation, the influx of 2DG-IR along the peri-arterial and peri-capillary space was visualized in astrocyte reporter mice (GLT1-eGFP). Cerebrospinal fluid (CSF) influx of glucose along the peri-vascular space mimics the delivery of glucose that cross the blood-brain-barrier: Glucose delivered by the vasculature or by CSF must in both cases pass the peri-vascular space before gaining access to neurons and astrocytes (Fig. 2a). Indeed, 2DG-IR was rapidly transported down along the peri-arterial and peri-capillary space. Real-time imaging showed that 2DG-IR moved quickly along the Virchow-Robin space and dispersed from the capillaries evenly into the parenchyma (Fig. 2b–c). We then assessed cellular 2DG-IR uptake in reporter mice *in vivo* (Fig. 2d). Neurons identified in CamKII-EGFP reporter mice displayed consistently higher 2DG-IR signal than surrounding neuropil, whereas the 2DG-IR signal in GLT1-eGFP^{+} astrocytes was either lower or did not differ from the surroundings (Fig. 2d). However, the high background signal of the untrapped 2DG-IR probe did not permit quantitative analysis of either neuronal or astrocytic 2DG-IR uptake.

Quantitative analysis shows that 2DG-IR uptake is highest in neurons

To obtain quantitative data of *in vivo* 2DG-IR uptake in neurons and astrocytes, we next developed an approach to image 2DG-IR signal in awake behaving mice with high cellular resolution: 2DG-IR was administered into CSF via injection into the cisterna magna to overcome the low blood-brain-barrier permeability of fluorescently-tagged glucose analogs. Cisterna magna injection also allowed analysis of multiple brain regions since CSF is distributed brain-wide distribution by the glymphatic system (Fig. 3a). As previously shown, CSF is rapidly pumped in along penetrating arteries and mixes with interstitial fluid by convective transport supported by astrocytic AQP4 channels (24, 25). Thirty minutes after CSF administration of 2DG-IR, the mice were perfusion-fixed and vibratome sections were prepared immediately. To reduce background signal, the slices were washed to remove

untrapped 2DG-IR (Fig. 3a). The use of GLT1-eGFP reporter mice in combination with nuclear labeling (yellow-Hoechst) enabled a side-by-side comparison of neuronal vs astrocytic 2DG-IR uptake. We took advantage of the observation that the diameter of neuronal nuclei (10.2 ± 0.7 μm) is 43.7% larger than that of astrocytes (7.1 ± 0.1 μm, p=0.01, t-test, N=3 mice) and defined neurons as cells with a round nuclei >9 μm and absence of eGFP (Fig. 3b). This *ex vivo* analysis showed that neurons throughout CNS, including cortex, striatum and hippocampal layers CA1 and CA3 exhibited on average 2.2-fold higher 2DG-IR uptake than astrocytes in awake mice (Fig. 3c–d). In particular, CA1 pyramidal neurons in hippocampus, which are metabolically highly active, displayed a 2.9-fold higher uptake of 2DG-IR than neighboring astrocytes.

Anesthesia predominantly supresses neuronal 2DG-IR uptake

We then explored the question of whether anesthesia differentially suppresses neuronal vs astrocytic energy metabolism. Initial experiments based on the classical quantitative autoradiographic measurements of ^{14}C-2DG confirmed that ketamine/xylazine anesthesia potently decreased cortical glucose utilization (Fig. 4a) (26–28). Interestingly, we found that ketamine/xylazine anesthesia also significantly decreased the ratio of neuronal vs astrocytic 2DG-IR uptake based on analysis of 2DG-IR signal in GLT1-EGFP reporter mice (Fig. 4b). Thus, anesthesia-induced suppression of glucose metabolism predominantly reflects a suppression of neuronal, rather than astrocytic, glucose uptake.

Sensory stimulation increases neuronal glucose uptake

In a revised version of the lactate shuttle hypothesis, it is proposed that activity-induced increases in glucose uptake reflect astrocytic glucose uptake and that astrocytes in turn produce lactate, which is oxidized by neurons (29). To test this hypothesis, we first evaluated how functional neuronal activation affects local 2DG-IR uptake. The mice were fasted prior to the experiment in order to reduce the potential effect of astrocytes' glycogen stores on cerebral metabolism (30–33). We stimulated the whiskers (3 Hz) unilaterally in awake mice and used local field potential (LFP) recordings to confirm that the whisker deflections induced neural responses in the contralateral barrel cortex for the duration of the stimulation period (Fig. 5a). We compared 2DG-IR uptake in ipsi- and contralateral sensory cortex and found that whisker stimulation significantly increased 2DG-IR uptake in contralateral compared with ipsilateral barrel cortex (Fig. 5b,d). A microscopic analysis of 2DG-IR uptake showed that whisker stimulation predominantly increased 2DG-IR uptake in neurons, since the ratio of 2DG-IR signal in neurons vs astrocytes increased from 2.1-fold to 3.3-fold in contra- vs ipsilateral barrel cortex of awake mice (P=0.006, t-test, Fig. 5e–g). In fact, 2DG-IR signal intensity in astrocytes did not exhibit an increase in contralateral barrel cortex compared with ipsilateral (41.3 ± 9.4 au in contralateral and 50.2 ± 8.8 in ipsilateral au, P=0.51, t-test, N=7 contralateral and N=9 ipsilateral). Analysis of glucose metabolism based on traditional ^{14}C-2DG autoradiography showed, in accordance with previous analysis, a significant increase in glucose consumption in the contralateral barrel cortex (19 ± 4%, P<0.01, t-test, Fig. 5c) (34). Thus, based on these observations, we conclude that sensory stimulation triggers an increase in glucose uptake preferentially by neurons.

Hexokinase expression is mainly neuronal and correlates with glucose consumption

From the astrocyte-to-neuron lactate shuttle hypothesis it follows that the level of glycolysis is required to be higher in astrocytes than neurons and thus hexokinases should be expressed preferentially in astrocytes. Gene expression analysis of FACS sorted pools of cortical neurons and astrocytes showed that both cell types express HK enzymes, as expected (33, 35, 36). However, the qPCR data of the mRNA revealed that the HK1, HK2, and HK3 genes were consistently expressed at a higher level in neurons than in astrocytes (Fig. 6a) (37). Using quantitative immunohistochemical analysis we confirmed the gene expression data: HK1, HK2 and HK3 immunolabeling were significantly higher in neurons than in astrocytes (Fig. 6b–k, Fig. 7a–e). The higher expression of the HK1-3 in neurons compared to astrocytes was not limited to cortex, but evident in all regions analyzed, including striatum and hippocampal layers CA1 and CA3 (Fig. 6b–k, Fig. 7a–e). Vascular endfeet of astrocytes were easily recognized in the GLT1-eGFP reporter mice and displayed, similarly to parenchymal astrocytes, low levels of HK (Fig. 6c–d). Thus, both qPCR and immunohistochemistry data suggested that the capacity for glucose phosphorylation, and therefore glycolysis, in neurons by far exceeds that of astrocytes. The observations that neurons take up more glucose and express several fold higher glycolytic enzymes (HK1-3) compared to astrocytes support the claim that neurons are the primary consumers of glucose (Fig. 6b–k, Fig. 7a–e). Plotting local glucose consumption as a function of local HK1 expression across several brain regions confirmed linear relationship (R^2=0.78, Fig. 8a–b) (17). Moreover, this observation was extended by the observation that the 2DG-IR uptake ratio for neurons vs astrocytes was also a function of local HK1 expression (R^2=0.85, Fig. 8c). These data emphasize the notion that hexokinase expression on a macroscopic level (comparing brain regions), as well as on a microscopic level (comparing different cell types) is a direct function of the basal level of glucose metabolism. Both the macro- and microscopic analysis of hexokinase expression suggested that glucose is primarily utilizes by neurons. Finally, we investigated the level of hexokinase 1, also called ‘brain hexokinase’, in adult human cortex (38). HK1 immunofluorescence signal was localized predominantly to $NeuN^+$ neurons, which consistently displayed stronger HK1 immunolabeling than GFAP positive astrocytes (Fig. 8d–e), supporting the hypothesis that glycolysis is an integral constituent of neuronal ATP production in both murine and human brain.

Discussion

In this study, we analyzed neuronal and astrocytic uptake of a near-infrared glucose analogue, 2DG-IR *in vivo* using 2-photon microscopy. Initial *in vitro* analysis validated that uptake of 2DG-IR follows similar uptake and inhibition kinetics as glucose and 2DG in both cultured neurons and astrocytes. The *in vitro* analysis also documented that neuronal uptake of glucose itself is 4-fold higher than astrocytes in cultures. *In vivo*, we delivered 2DG-IR directly into CSF of awake behaving reporter mice to visualize cellular 2DG-IR uptake. Real-time imaging showed that 2DG-IR entered cortex along penetrating arteries and reached the capillary bed by convective transport along the perivascular space, followed by uptake by both neurons and astrocytes. Quantitative analysis of cellular 2DG-IR uptake indicated that the glucose analogue was preferentially taken up by neurons in awake

animals, and that ketamine/xylazine anesthesia predominantly suppressed neuronal glucose metabolism. Also, whisker stimulation increased neuronal, rather than astrocytic, 2DG-IR in awake mice. Thus, our analysis showed that neurons consistently take up more glucose than astrocytes across several fundamentally different states of brain activity. Another important conclusion is that glucose metabolism should be studied in awake rather than anesthetized animals, since anesthesia preferentially suppressed neuronal 2DG-IR uptake.

Hexokinases are housekeeping enzymes that catalyze the first step of glycolysis (35, 36). Analysis of gene expression in FACS sorted neuron and astrocytes showed that all 3 isoforms of hexokinase (HK1-3) are expressed at higher levels in neurons than astrocytes. A quantitative immunohistochemical analysis confirmed and extended this observation by showing that HK1-3 are present at a higher levels in neurons than astrocytes in all brain regions analyzed. The enrichment of HK1 in NeuN-positive neurons is in agreement with the observation that 40–50% of HK activity is localized in synaptosomes (39). We also confirmed that regional HK1 expression correlates with local glucose utilization (17), and extended this observation to demonstrate that the ratio of neuron/astrocyte glucose uptake correlates with HK1 content in the same regions. In human cortex, an assessment of the prevailing hexokinase, HK1 (38, 40), revealed a much stronger HK1 immunolabeling of $NeuN^+$ neurons than $GFAP^+$ astrocytes, suggesting that our observations in mice can be extended to human brain. An additional important observation was that HK1 was not enriched in vascular endfeet of astrocytes, as would expected according to the astrocyte-to-neuron lactate shuttle hypothesis. Combined, our observations are consistent with the simple model that neurons, rather than astrocytes, are the primary direct consumers of glucose.

The CNS consumes 10-fold more energy than the average of peripheral tissue and relies almost exclusively on glucose as energy substrate (20, 41, 42). According to the astrocyte-neuron lactate shuttle hypothesis, glucose uptake is delegated to astrocytes and neurons chiefly rely on import of lactate from nearby astrocytes. The concept of the astrocyte-to-neuron lactate shuttle was originally based on the observation that glutamate uptake in cultured astrocytes activated aerobic glycolysis leading to an increased astrocytic production of lactate (8). Accordingly, glutamatergic signaling enhances astrocytic lactate production and lactate is in turn imported and oxidized by neurons. Several experiments have in the past supported the existence of astrocyte-to-neuron lactate shuttle hypothesis (4, 6, 8, 29). *In vitro* studies have used shorter wavelength glucose analogues, including 2-NBDG and 6-NBDG, to compare the uptake kinetics in cultured neurons and astrocytes (22). However, comparison of transport kinetic in different cell types is complicated, because the glucose transporter isoforms differ with regard to affinity and transport kinetics (19). Neurons express primarily GLUT3 whereas GLUT1 is highly enriched in astrocytes (18, 19). One prior study assessed 2-NBDG accumulation *in vitro*, rather than its transport kinetics, and concluded that the glucose analogue is primarily taken up by neurons, consistent with our findings (43, 44). Data collected in brain slices incubated with fluorescent glucose analogues have also supported the astrocyte-to-neuron lactate shuttle hypothesis (45, 46). However, interpretation of the slice data is difficult, as glucose is not delivered by the vasculature and astrocytes rapidly acquire a reactive phenotype *ex vivo* (47). An analysis based on *in vivo* imaging of the glucose analogue, 6NBDG, at rest and during functional activation in

anesthetized mice concluded, as opposed to our study, that neurons take up more glucose than atsrocytes (48). However, C6-conjugated glucose analogues cannot be phosphorylated by the hexokinases (which target the C6 site occupied by the fluorescent tag), as opposed to the classical glucose analogues used to assess glucose consumption, including the 2DG derivative, ^{18}FDG, 2NBDG, or 2DG-IR. Consequently, 6NBDG is not trapped within the cells rendering it is difficult to compare neuronal versus astrocytic uptake (26, 49). Definitive proofs for or against the existence of the astrocyte-to-neuron lactate shuttle *in vivo*, have also been hampered by the lack of cellular resolution of the classical autoradiographic analysis of radiolabeled 2DG (50). Two prior studies attempted to overcome this limitation by applying emulsion directly on the sections. Albeit the majority of the grains were located over large cell bodies, consistent with the high hexokinase expression in neuronal cell bodies, the lack of immunolabeling prevented definitive cell identification (12, 51).

The glucose analogue used in this study, 2DG-IR, was developed for infrared non-invasive imaging of tumors with high glucose consumption (13, 14). Long wavelength excitation and emission has several advantages, including better tissue penetration, less scattering, and low autofluorescence. 2DG-IR has, to our knowledge, not previously been employed in analysis of cerebral metabolism. We took advantage of that small tracers are rapidly distributed brain-wide by convective fluxes of CSF to bypass the poor permeability of fluorescently-tagged glucose analogs across the blood-brain barrier (BBB) (25). Our analysis confirmed that 2DG-IR within minutes was transported along the peri-arterial and peri-capillary space and shortly thereafter distributed evenly across all brain regions. In fact, delivery of glucose analogues by convective CSF influx via the glymphatic system closely replicates vascular delivery of glucose, because both pathways require that the glucose tracers crosses the peri-capillary space prior to gaining access to either astrocytes and neurons. The even distribution of 2DG-IR across all brain regions suggest that cisterna magna injection of agents with poor BBB permeability also may be a useful tool for other studies that requires brain-wide distribution including pharmacological manipulations, loading of fluorescent indicators or viral transfection. We perfusion-fixed the mice 30 min after *in vivo* 2DG-IR administration and prepared vibratome sections immediately thereafter. The 2DG-IR signal in intact cells was collected using 1280 nm excitation in the slices. The intactness of the plasma membrane following perfusion-fixation was, in pilot experiments, evaluated by imaging the same field repeated over a period of 24 hrs. This analysis showed that the cellular signals did not change significantly over time suggesting that the intact plasma membrane prevented diffusion of the glucose analogue trapped within the plasma membrane. This observation is in agreement with earlier studies, in which fine cellular structures were visualized by intracellular injection of fluorescent indicators in freshly cut perfusion-fixed slices (52). We also used transgenic reporter mice (GLT1-eGFP) to positively label astrocytes and yellow Hoechst to identify surrounding neurons based on the large size of the neuronal nuclei, as well as the loose chromatin structure with multiple nucleoli, and lack of eGFP. Combined, these technical advances improved the cellular details of the 2DG-IR signal and allowed with high specificity quantification of glucose uptake in neurons and astrocytes located next to each other across multiple brain regions and 3 different states of brain activity.

Our analysis confirms a recent study in anesthetized rats, which showed that bicuculline-induced seizures increased ^{18}F-DG phosphorylation in isolated nerve terminals, suggesting that local neuronal glycolysis supports increased synaptic activity (11). The activity of hexokinases is inhibited by ATP and the product of their own reaction, glucose-6-phosphate, and it has been estimated that hexokinase activity is 97% inhibited at rest (53). Thus, a decline in cytosolic ATP and glucose-6-phosphate in rapidly spiking neurons may drive neuronal, rather than astrocytic, glucose consumption during functional activation. This conclusion is of importance, because metabolic surrogates of metabolism are widely employed in functional imaging studies (54–57). However, interpretation of functional autoradiographic and PET studies based on radiolabeled (^{14}C or ^{3}H) 2DG and ^{18}FDG, respectively, have been complicated by the astrocyte-to-neuron lactate shuttle hypothesis. The data presented here provides insight into the cellular basis for functional brain imaging, by showing that glucose is taken up by neurons in an activity-dependent manner and that regional 2DG or ^{18}FDG accumulation thereby can be used as direct measure of neuronal activity. In future experiments, imaging glucose uptake based on administration of 2DG-IR in the CSF provides a new experimental approach to dissect cellular metabolic responses to state-dependent changes in neural activity, or pathological conditions such as ischemia, epilepsy, or accumulation of protein aggregates in neurodegenerative diseases.

Materials and methods

Mice

All mice were 2–3 months old (~25 g) unless otherwise stated. CamkIIa-CreERT2/CAG-tdTomato (CamkIIa-tdTomato) mice were generated by crossing B6.129S6-Tg (CamkIIa-cre/ERT2)1Aibs/J mice and B6.Cg-*Gt(ROSA)26Sor*$^{tm14(CAG-tdTomato)Hze}$/J (Jackson) (58–60). At 5-week old, tamoxifen (Sigma; T5648) was injected (150 mg/kg, i.p.) daily for seven consecutive days. BAC GLT1-eGFP (GLT1-eGFP) (61) mice were used as astrocyte reporter mice. All strains were maintained on C57BL/6J background and C57BL/6NCrl mice were purchased from Charles River Laboratory to rejuvenate the transgenic lines. All experiments were approved by the University Committee on Animal Resources of the University of Rochester and carried out according to guidelines from the National Institute of Health.

Fluorescence-activated cell sorting and RNA extraction

8 weeks old CamkIIa-tdTomato and GLT1-eGFP mice were used for isolating neurons and astrocytes respectively. Preparation of single cell suspension from mouse cortex and hippocampus and fluorescence-activated cell sorting (FACS) were performed as described previously (37, 62). Cortical tissue from 3 mice was pooled for one sample, with a yield of 4~8×10^{6} cells per mouse. A 561 nm and 488 nm laser was used for tdTomato and eGFP excitation respectively, and emissions were collected by a 610/20 nm and 530/30 nm band-pass filter, respectively. Cells were sorted into either tdTomato^{+} (neurons) and tdTomato^{-}, or eGFP^{+} (astrocytes) and eGFP^{-} populations. RNA of FACS sorted cells was extracted using RNeasy Micro Kit (Qiagen) (37).

Quantitative PCR (qPCR)

For qPCR, total RNA was reverse transcribed and amplified using Ovation PicoSL WTA System V2 (NuGEN). Relative quantity of transcripts was assessed using Taqman Assays on Demand and a 7000 Sequence Detection System. Expression of Synaptosomal-associated protein 25 (Snap25) and Embryonic Lethal Abnormal Vision Drosophila-Like 4 (Elav4) in neurons, Solute Carrier Family 1, Member 2 (Slc1a2) and Aquaporin 4 (Aqp4) in astrocytes and the absence of Integrin, Alpha M (Itgam, microglia) and myelin oligodendrocyte glycoprotein (Mog, oligodendrocytes) expression were used to verify sorting specificity. RNA quantity was normalized to glyceraldehyde 3-phosphate dehydrogenase (GAPDH) before calculating relative expression of target genes (63). Values were expressed as log2 of the ratio of the relative expression ratio of target gene in $CamkIIa^+/CamkIIa^-$ or $GLT1^+/GLT1^-$ cells.

Cell cultures

Neocortical astrocyte cultures were prepared from 1–2 days old GLT1-eGFP mice (64). Astrocytes were plated in 25 cm^2 culture flask (10^6 cells/flask) and maintained in 10% fetal bovine serum in Dulbecco's modified Eagle's medium (DMEM)/F12, containing penicillin (100 IU/ml) and streptomycin (100 μg/ml). When the cultures became confluent, the cells were re-plated in 24-well plates (2×10^5 cell/well). Experiments were performed when the cells were 90% confluent, about 2 days after seeding down. Neocortical neuronal cultures were prepared from 1–5 days old C57BL/6 mice as previously described (64). The cells were seeded onto poly-D-lysine–coated 24-well plates (10^5 cells/well) and maintained in Neurobasal A medium (Invitrogen) with 2% B27, 0.5 mM GlutaMAX, gentamycin (10 μg/ml), and human fibroblast growth factor 2 (FGF2, 5 ng/ml). Neuronal cultures were used 7 days after plating. More than 95% of the cells stained positive for GFAP in the astrocyte cultures and more than 95% of the cells stained positive for PSA-NCAM in the neuronal cultures (see method section for immunohistochemistry, microscopy, and image analysis).

Cell culture assays

Neuron and astrocyte cultures, 90% confluent, in 24-well plates were washed twice and pre-incubated in 0.5 mM D-glucose (Sigma) in DMEM for 30 min at 37°C (64, 65). The assay media contained 0.5 mM D-glucose and D[U-^{14}C]-glucose (^{14}C-glucose) or glucose analogs 2[^{14}C(U)-deoxy-D-glucose (^{14}C-2DG) or IRDye 800CW-2-deoxyglucose (2DG-IR, LI-COR Biosciences, Nebraska, USA) in DMEM (8, 66). All experiments were performed at 37°C. At the end of the experiment the cells were washed three times with 0.5 mL ice-cold glucose-free DMEM containing 0.5 mM glucose. For ^{14}C-glucose and ^{14}C-2DG experiments 1 μCi/ml (0.5 mM, PerkinElmer, MA, USA) was used and at the end of the experiment the cells were lysed in 200 μL 0.5 N NaOH/0.1% Triton X-100. Protein concentration was determined by Pierce® BCA protein assay kit (Thermo Scientific). ^{14}C radioactivity was quantified using a liquid scintillation counter (Beckman Coulter, LS6500 Scintillation Counter, GA, USA). For 2DG-IR uptake experiments assays were performed in 96 well plates with 100 μM 2DG-IR in the assay media. After incubation with 2DG-IR, followed by 3 quick washes, 2DG-IR signal was imaged in 3 random places per well using a 20× water immersion lens (0.95 NA). Mean pixel intensity was measured using NIH ImageJ

1.47v software and background intensity measurement (blank well with media) was subtracted. Assay times for ^{14}C-glucose, ^{14}C-2DG and 2DG-IR were 1, 2, 6, or 10 min. The initial rate of uptake was determined by linear regression analysis from the initial linear phase of the uptake vs time graph. Uptake inhibition experiments with addition of D-glucose (in mM: 0, 0.1, 0.2, 0.3, 1, 3, 10, 30, 100, 300, Sigma) or cytochalasin B (in μM: 0, 1, 5, 10, 20, 40, Sigma) to the assay media, DMEM containing 0.5 mM D-glucose, were performed at 1 min. For 2DG-IR competition and inhibition experiments, 10 μM 2DG-IR was added to the assay media and the well plate was imaged using an IVIS® spectrum imaging system (Caliper Life Science, MA, USA), and the mean fluorescence signal was used. Uptake of ^{14}C-glucose and ^{4}C-2DG was expressed as nmol/mg protein, 2DG-IR was expressed as the mean fluorescence intensity. The inhibitory constant, Ki, was calculated using Graph Pad Prism 5. All experiments were performed in triplicate.

Immunohistochemistry, microscopy, and image analysis

Immunohistochemistry was performed as previously described (67). The primary antibodies used were: mouse anti-hexokinase (HK) 1 (1:250, Millipore MAB1534), rabbit anti-HK2 (Millipore AB3279, 1:200), rabbit anti-HK3 (Santa Cruz sc-28890, 1:100), mouse anti-NeuN (Chemicon MAB377, 1:200), rabbit anti-NeuN (Millipore ABN78, 1:250), rabbit anti-GFAP (DAKO Z0334, 1:250), mouse anti-PSA-NCAM (Millipore MAB5324, 1:250). Alexa Fluor-conjugated secondary antibodies were incubated for 2 hours at RT (Life Technologies, 1:500). DAPI (Sigma, 1:2000) was used to identify cell nuclei. For immunohistochemistry on human tissue, the tissue was immersion-fixed in 4% PFA, embedded in O.C.T. Tissue-Tek (Sakura) and cut in 20 μm cryostat sections. A biotinylated secondary antibody (1:200) directed against HK1 primary antibody was used. Alexa Fluor-conjugated streptavidin (20 μg/mL) was applied for 2 hrs. Immunofluorescence was visualized using a Bio-Rad MRC500 confocal scanning microscope attached to an inverted microscope (IX81, Olympus, Tokyo, Japan) controlled by Olympus Fluoview 500 software. A 4× lens (0.16 NA) was used to image HK immunofluorescence for comparison of different brain regions, a 10× lens (0.3 NA) was used for imaging of immunocytochemistry, a 40× lens (1.3 NA) was used for imaging of immunocytochemistry for cellular HK quantification and a 100× lens (1.3 NA) was used for Z-stacks. A Z-stack of 0.1 μm steps was acquired for orthogonal projections (xz, yz plane). Orthogonal projections were made using Olympus Fluoview 500 software (47). For analysis of hexokinase protein immunohistochemistry was performed on 100 μm vibratome slices of GLT1-eGFP mice. Neurons were identified by NeuN-labeling. Astrocytes were identified by eGFP expression. NIH ImageJ software 1.47v was used to measure hexokinase 1 (HK1) immunoreacticity intensity. The intensity of HK1 immunoreactivity in the nucleus (co-localization with DAPI) was subtracted from the HK1 intensity in the soma to yield the cytoplasmic HK1 immunoreactivity intensity. Background intensities (>3 per image) were measured in cell-free parenchyma in the same field of view and the data was displayed as the percentage difference between in neuronal and astrocytic fluorescence intensity, respetively, compared to cell-free parenchyma. Cell-free parenchyma was defined as space devoid of eGFP, NeuN or DAPI but could contain some unidentified cellular processes of e.g. astrocytes or neurons. A total of 30–50 neurons and 30–50 astrocytes per brain region were quantified in N=4

mice. For comparison of HK immunoreactivity in different brain regions images were normalized to the intensity measure in the cortex of each sample (N=5).

Awake whisker stimulation and electrophysiological recording

Adult GLT1-eGFP mice underwent adaptive behavioral training for awake restraining using several 1 hr sessions over two consecutive days. The mice were fasted over night before the day of the experiment. Whiskers were trimmed to 10-mm length and stimulated by air puffs (68). The tube for air puffing was placed parallel to the left side of the mouse snout 15–20 mm in front of the C6 whisker. Air puffs controlled by a picospritzer (Parker Instrumentation) were generated at 3 Hz, 20 psi, 10 msec pulses for a duration of 30 min. Local field potential (LFP) recordings were obtained from primary sensory cortex (100–150 μm below the pial surface) by a patch pipette (TW100F-4, WPI; outer diameter, 1.0 mm; inner diameter, 0.75 mm; tip diameter, 3 μm), containing artificial cerebrospinal fluid (ACSF) containing (in mM): 126 NaCl, 2.5 KCl, 1.25 NaH_2PO_4, 2 $MgCl_2$, 2 $CaCl_2$, 10 glucose and 26 $NaHCO_3$ (pH 7.4). LFP signals were amplified by a MultiClamp 700B (Axon Instruments), bandpass filtered at (1–100 Hz) and digitized at 10 kHz (68).

Animal preparation for *in vivo* 2-photon imaging

GLT1-eGFP mice and CamkIIa-tdTomato mice were anesthetized with 2% isoflurane in 2 L O_2/min and a custom made metal plate was glued to the skull with dental acrylic cement. The mice were habituated to the microscope stage over the following 2 days by several training session each lasting 30–60 min. At day 2 the mice were fasted over night. At day 3, the mice were anesthetized with 2% isoflurane and a cranial window was prepared over the right hemisphere at 2.5 mm lateral and 2 mm posterior to bregma. The dura was left intact and the craniotomy (~3 mm diameter) was covered with 1.5% agarose (type III-A, Sigma) and a glass coverslip, and then sealed with dental cement. All mice were allowed to recover for 4–6 hrs prior to imaging. In awake mice and mice anesthetized with ketamine/xylazine (KX, 100 mg/kg, 10 mg/kg, i.p.) 2DG-IR was micro-injected along a penetrating arteriole in the cortex at a concentration of 1 mM using a fine glass electrode connected to a picospritzer (1 Hz, 10 psi, 100 ms pulses, for 10 min; Parker Instrumentation). To visualize the vasculature, the BBB impermeable Texas Red-dextran (70 kD, 1% in saline) or FITC-dextran (2,000 KDa, 1% in saline) was injected into the femoral vein of GLT1-eGFP mice and CamkIIa-tdTomato mice, respectively.

Quantification of cellular 2DG-IR uptake *in vivo*

Adult (>2 months old) GLT1-eGFP mice were used for 2DG-IR experiments. In one group the mice were anesthetized with KX, in another group the mice were awake. All awake mice received behavioral training described in the whisker stimulation section and all mice were fasted over night before the experiment. The mice were infused with 20 μl of 1 mM 2DG-IR into cisterna magna (2 μl/min). Whisker stimulation was initiated simultaneously with the start of 2DG-IR injection. The mice were perfused with 4% paraformaldehyde (PFA) after 30 min. For comparison of 2DG-IR uptake by neurons and astrocytes, the brains were immediately sectioned in 100 μm thick slices using vibratome, incubated with 40 μM yellow Hoechst in PBS (Life Technologies; S769121) for 20 min, washed twice in PBS for 10 min and mounted on a glass slide in Prolong (Invitrogen). All images were acquired using 2-

photon imaging with the same photomultiplier tube setting and gain for 2DG-IR within 2–3 hrs after perfusion fixation. Astrocytes were identified by cytosolic eGFP signal. Neurons were identified by their lack of eGFP and as cells with a round, lightly stained nuclei of >9 μm in size (Fig. 3b). A quantitative analysis showed that $NeuN^+$ nuclei were on average 43.7% larger in diameter than nuclei of GLT1-$eGFP^+$ astrocytes (10.2 ± 0.7 μm for neurons, 7.1 ± 0.1 μm for astrocytes, P=0.01, t-test, 82 neurons and 26 astrocytes quantified in N=3 mice). Measurements of 2DG-IR intensity were performed using NIH ImageJ 1.47v software. 2DG-IR background signal (measured in parenchyma) in the same field was subtracted from intensity measures in neurons and astrocytes in each image. In cortex the total number of neurons and astrocytes analyzed, was 333 and 125 for KX, 431 and 164 for awake/ipsilateral and 387 and 140 for contralateral cortex, respectively. For analyses of other areas, 162 ± 22 neurons and 59 ± 4 astrocytes were analyzed per mouse in N=7–8 mice. For imaging of 2DG-IR uptake in whole slices, an IVIS® spectrum imaging system (Caliper Life Science, MA, USA) was used with an excitation and emission wavelength of 745 nm and 795 nm, respectively. A set of 20 images of whole brain section was collected for each section and merged to generate a higher resolution final image. 2DG-IR content in the ipsilateral and contralateral barrel cortex and thalamus were quantified using NIH ImageJ software 1.47v.

2-photon imaging

A Chameleon Ti:Sapphire laser (Coherent, Glasgow, UK) connected to a Chameleon compact opo system was controlled by Olympus Fluoview FV500 software (25). A 20× water immersion lens (0.95 NA) was used for *in vivo* and slice imaging. eGFP, 2,000 KDa dextran-FITC, 70 KDa dextran-Texas Red and yellow Hoechst were excited using a 900 nm laser. An 800 nm laser was tuned to 1280 nm by the opo system for 2DG-IR excitation. Bandpass filters (Chroma) were 540/40 for eGFP and FITC, 650/75 nm for yellow Hoechst, 675/65 nm for tdTomato and Texas Red and 855/210 nm for 2DG-IR emission. Single channel acquisition was used for 2DG-IR and dual channel acquisition was used for combination of other fluorophores.

^{14}C autoradiography

Awake or KX-anesthetized adult male C57BL/6 mice (25 g) were injected with ^{14}C-2DG (5 μCi/mouse, bolus) into the femoral vein. All mice were fasted over night before the day of the experiment. Arterial blood samples (20 μL/sample) were collected before the injection for glucose determination and after the injection (11 samples during the experiment) for plasma radioactivity analysis. Total plasma glucose was determined using a kit (GAHK-20, Sigma). At the end of the experiments mice were decapitated and their brains were embedded in O.C.T. Tissue-Tek (Sakura). Coronal sections (20 μm) were cut using a cryostat, collected on specimen glass slides, dried and exposed to autoradiographic film (Amersham Hyperfilm, GE Healthcare, UK) for 12 days with a ^{14}C- standard (American Radiolabeled Chemicals Inc, MO, USA). Intensity measurements of the developed films were performed using NIH ImageJ software 1.47v. Glucose utilization (μmol/100g/min) was determined as: (Cp/LC) $[C^*(T)-k_1^*A]/[B-A]$, where Cp is the plasma glucose concentration in mM, LC is the lump constant, $C^*(T)=^{14}C$-2DG in brain region at time T, k_1^*,k_2^* and k_3^*

are the influx, efflux and phosphorylation rate constants of ^{14}C-2DG, $A=e^{-Kt}\int_0^T C^*_p(t)e^{Kt}dt$, $B=\int_0^T C_p^*(t)dt$, $K=k_2^*-k_3^*$ (26–28, 49, 69).

Statistics

Values were expressed as mean ± s.e.m. An unpaired student's t-test was used for pairwise comparisons. A paired t-test was used for analysis of neuronal 2DG-IR uptake normalized to astrocytic uptake in the same area. A Mann-Whitney test was used for pairwise comparison of data that did not follow normal distribution. ANOVA analysis with Tukey-Kramer post hoc test was used for comparisons of more than two groups. All statistics were performed using GraphPad Prism 5.

Acknowledgements

This work was supported by NIH/NINDS and Lundbeck Foundation. We thank Weiguo Peng, Yonghong Liao, and Thiyagarajan Meenakshisundaram for expert technical assistance. GLT1-eGFP mice were kindly donated by Jeff Rothstein.

References

1. Dienel GA, Hertz L. Glucose and lactate metabolism during brain activation. Journal of neuroscience research. 2001; 66:824–838. [PubMed: 11746408]
2. Hertz L, Dienel GA. Energy metabolism in the brain. International review of neurobiology. 2002; 51:1–102. [PubMed: 12420357]
3. Pellerin L, et al. Evidence supporting the existence of an activity-dependent astrocyte-neuron lactate shuttle. Developmental neuroscience. 1998; 20:291–299. [PubMed: 9778565]
4. Magistretti PJ, Pellerin L, Rothman DL, Shulman RG. Energy on demand. Science. 1999; 283:496–497. [PubMed: 9988650]
5. Pellerin L, Magistretti PJ. Food for thought: challenging the dogmas. Journal of cerebral blood flow and metabolism : official journal of the International Society of Cerebral Blood Flow and Metabolism. 2003; 23:1282–1286.
6. Belanger M, Allaman I, Magistretti PJ. Brain energy metabolism: focus on astrocyte-neuron metabolic cooperation. Cell metabolism. 2011; 14:724–738. [PubMed: 22152301]
7. Wyss MT, Jolivet R, Buck A, Magistretti PJ, Weber B. In vivo evidence for lactate as a neuronal energy source. The Journal of neuroscience : the official journal of the Society for Neuroscience. 2011; 31:7477–7485. [PubMed: 21593331]
8. Pellerin L, Magistretti PJ. Glutamate uptake into astrocytes stimulates aerobic glycolysis: a mechanism coupling neuronal activity to glucose utilization. Proceedings of the National Academy of Sciences of the United States of America. 1994; 91:10625–10629. [PubMed: 7938003]
9. Gjedde A, Marrett S. Glycolysis in neurons, not astrocytes, delays oxidative metabolism of human visual cortex during sustained checkerboard stimulation in vivo. Journal of cerebral blood flow and metabolism : official journal of the International Society of Cerebral Blood Flow and Metabolism. 2001; 21:1384–1392.
10. Mangia S, Simpson IA, Vannucci SJ, Carruthers A. The in vivo neuron-to-astrocyte lactate shuttle in human brain: evidence from modeling of measured lactate levels during visual stimulation. Journal of neurochemistry. 2009; 109(Suppl 1):55–62. [PubMed: 19393009]
11. Patel AB, et al. Direct evidence for activity-dependent glucose phosphorylation in neurons with implications for the astrocyte-to-neuron lactate shuttle. Proceedings of the National Academy of Sciences of the United States of America. 2014; 111:5385–5390. [PubMed: 24706914]
12. Nehlig A, Wittendorp-Rechenmann E, Lam CD. Selective uptake of [14C]2-deoxyglucose by neurons and astrocytes: high-resolution microautoradiographic imaging by cellular 14C-trajectography combined with immunohistochemistry. Journal of cerebral blood flow and

metabolism : official journal of the International Society of Cerebral Blood Flow and Metabolism. 2004; 24:1004–1014.

13. Kovar JL, Volcheck W, Sevick-Muraca E, Simpson MA, Olive DM. Characterization and performance of a near-infrared 2-deoxyglucose optical imaging agent for mouse cancer models. Analytical biochemistry. 2009; 384:254–262. [PubMed: 18938129]
14. Zhou H, et al. Dynamic near-infrared optical imaging of 2-deoxyglucose uptake by intracranial glioma of athymic mice. PloS one. 2009; 4:e8051. [PubMed: 19956682]
15. Dienel GA. Fueling and imaging brain activation. ASN neuro. 2012; 4
16. McKenna MC. Substrate competition studies demonstrate oxidative metabolism of glucose, glutamate, glutamine, lactate and 3-hydroxybutyrate in cortical astrocytes from rat brain. Neurochemical research. 2012; 37:2613–2626. [PubMed: 23079895]
17. Turek TJ, Hawkins RA, Wilson JE. Correlation of hexokinase content and basal energy metabolism in discrete regions of rat brain. Journal of neurochemistry. 1986; 46:983–985. [PubMed: 3512776]
18. Gerhart DZ, LeVasseur RJ, Broderius MA, Drewes LR. Glucose transporter localization in brain using light and electron immunocytochemistry. Journal of neuroscience research. 1989; 22:464–472. [PubMed: 2668543]
19. Vannucci SJ, Maher F, Simpson IA. Glucose transporter proteins in brain: delivery of glucose to neurons and glia. Glia. 1997; 21:2–21. [PubMed: 9298843]
20. Kennedy C, et al. Mapping of functional neural pathways by autoradiographic survey of local metabolic rate with (14C)deoxyglucose. Science. 1975; 187:850–853. [PubMed: 1114332]
21. Reivich M, et al. Measurement of local cerebral glucose metabolism in man with 18F-2-fluoro-2-deoxy-d-glucose. Acta neurologica Scandinavica. Supplementum. 1977; 64:190–191. [PubMed: 268783]
22. Barros LF, et al. Kinetic validation of 6-NBDG as a probe for the glucose transporter GLUT1 in astrocytes. Journal of neurochemistry. 2009; 109(Suppl 1):94–100. [PubMed: 19393014]
23. Tucker SP, Cunningham VJ. Autoradiography of [3H]cytochalasin B binding in rat brain. Brain research. 1988; 450:131–136. [PubMed: 2841000]
24. Iliff JJ, et al. A paravascular pathway facilitates CSF flow through the brain parenchyma and the clearance of interstitial solutes, including amyloid beta. Science translational medicine. 2012; 4:147ra111.
25. Xie L, et al. Sleep drives metabolite clearance from the adult brain. Science. 2013; 342:373–377. [PubMed: 24136970]
26. Toyama H, et al. Absolute quantification of regional cerebral glucose utilization in mice by 18F-FDG small animal PET scanning and 2-14C-DG autoradiography. Journal of nuclear medicine : official publication, Society of Nuclear Medicine. 2004; 45:1398–1405.
27. Nedergaard M, Gjedde A, Diemer NH. Focal ischemia of the rat brain: autoradiographic determination of cerebral glucose utilization, glucose content, and blood flow. Journal of cerebral blood flow and metabolism : official journal of the International Society of Cerebral Blood Flow and Metabolism. 1986; 6:414–424.
28. Nedergaard M, Jakobsen J, Diemer NH. Autoradiographic determination of cerebral glucose content, blood flow, and glucose utilization in focal ischemia of the rat brain: influence of the plasma glucose concentration. Journal of cerebral blood flow and metabolism : official journal of the International Society of Cerebral Blood Flow and Metabolism. 1988; 8:100–108.
29. Bouzier-Sore AK, Merle M, Magistretti PJ, Pellerin L. Feeding active neurons: (re)emergence of a nursing role for astrocytes. Journal of physiology, Paris. 2002; 96:273–282.
30. Suzuki A, et al. Astrocyte-neuron lactate transport is required for long-term memory formation. Cell. 2011; 144:810–823. [PubMed: 21376239]
31. Cruz NF, Dienel GA. High glycogen levels in brains of rats with minimal environmental stimuli: implications for metabolic contributions of working astrocytes. Journal of cerebral blood flow and metabolism : official journal of the International Society of Cerebral Blood Flow and Metabolism. 2002; 22:1476–1489.
32. Phillips ME, Coxon RV. The relative constancy of the glycogen content of guinea pig brain. Journal of neurochemistry. 1973; 20:1295–1297. [PubMed: 4697891]

33. Dienel GA. Astrocytes are 'good scouts': being prepared also helps neighboring neurons. Journal of cerebral blood flow and metabolism : official journal of the International Society of Cerebral Blood Flow and Metabolism. 2010; 30:1893–1894.
34. Ravasi L, et al. Use of [18F]fluorodeoxyglucose and the ATLAS small animal PET scanner to examine cerebral functional activation by whisker stimulation in unanesthetized rats. Nuclear medicine communications. 2011; 32:336–342. [PubMed: 21326123]
35. Lai JC, Behar KL, Liang BB, Hertz L. Hexokinase in astrocytes: kinetic and regulatory properties. Metabolic brain disease. 1999; 14:125–133. [PubMed: 10488914]
36. Snyder CD, Wilson JE. Relative levels of hexokinase in isolated neuronal, astrocytic, and oligodendroglial fractions from rat brain. Journal of neurochemistry. 1983; 40:1178–1181. [PubMed: 6834050]
37. Sun W, et al. Glutamate-dependent neuroglial calcium signaling differs between young and adult brain. Science. 2013; 339:197–200. [PubMed: 23307741]
38. Wilson JE. Isozymes of mammalian hexokinase: structure, subcellular localization and metabolic function. The Journal of experimental biology. 2003; 206:2049–2057. [PubMed: 12756287]
39. Wilson JE. The localization of latent brain hexokinase on synaptosomal mitochondria. Archives of biochemistry and biophysics. 1972; 150:96–104. [PubMed: 4337541]
40. Grossbard L, Schimke RT. Multiple hexokinases of rat tissues. Purification and comparison of soluble forms. The Journal of biological chemistry. 1966; 241:3546–3560. [PubMed: 5919684]
41. Himwich H, Nahum L. Respiratory quotient of brain. Amer J Physiol. 1929; 90:389–396.
42. Siesjo, BK. A Wiley-Interscience publication. New York: John Wiley & Sons; 1978. Brain Energy Metabolism.
43. Pancani T, Anderson KL, Porter NM, Thibault O. Imaging of a glucose analog, calcium and NADH in neurons and astrocytes: dynamic responses to depolarization and sensitivity to pioglitazone. Cell calcium. 2011; 50:548–558. [PubMed: 21978418]
44. Itoh Y, Abe T, Takaoka R, Tanahashi N. Fluorometric determination of glucose utilization in neurons in vitro and in vivo. Journal of cerebral blood flow and metabolism : official journal of the International Society of Cerebral Blood Flow and Metabolism. 2004; 24:993–1003.
45. Jakoby P, et al. Higher transport and metabolism of glucose in astrocytes compared with neurons: a multiphoton study of hippocampal and cerebellar tissue slices. Cerebral cortex. 2014; 24:222–231. [PubMed: 23042735]
46. Barros LF, et al. Preferential transport and metabolism of glucose in Bergmann glia over Purkinje cells: a multiphoton study of cerebellar slices. Glia. 2009; 57:962–970. [PubMed: 19062182]
47. Takano T, et al. Rapid manifestation of reactive astrogliosis in acute hippocampal brain slices. Glia. 2014; 62:78–95. [PubMed: 24272704]
48. Chuquet J, Quilichini P, Nimchinsky EA, Buzsaki G. Predominant enhancement of glucose uptake in astrocytes versus neurons during activation of the somatosensory cortex. The Journal of neuroscience : the official journal of the Society for Neuroscience. 2010; 30:15298–15303. [PubMed: 21068334]
49. Sokoloff L, et al. The [14C]deoxyglucose method for the measurement of local cerebral glucose utilization: theory, procedure, and normal values in the conscious and anesthetized albino rat. Journal of neurochemistry. 1977; 28:897–916. [PubMed: 864466]
50. Chih CP, Roberts EL Jr. Energy substrates for neurons during neural activity: a critical review of the astrocyte-neuron lactate shuttle hypothesis. Journal of cerebral blood flow and metabolism : official journal of the International Society of Cerebral Blood Flow and Metabolism. 2003; 23:1263–1281.
51. Hokfelt T, et al. Improved resolution of the 2-deoxy-D-glucose technique. Brain research. 1983; 289:311–316. [PubMed: 6661649]
52. Bushong EA, Martone ME, Jones YZ, Ellisman MH. Protoplasmic astrocytes in CA1 stratum radiatum occupy separate anatomical domains. The Journal of neuroscience : the official journal of the Society for Neuroscience. 2002; 22:183–192. [PubMed: 11756501]
53. Clarke, D.; Lajitha, A.; Maker, H. Basic Neurochemistry. fourth edn. New York: Raven Press; 1989. p. 542-550.vol.

54. Phelps ME, Mazziotta JC, Huang SC. Study of cerebral function with positron computed tomography. Journal of cerebral blood flow and metabolism : official journal of the International Society of Cerebral Blood Flow and Metabolism. 1982; 2:113–162.
55. Ward NS, Frackowiak RS. Towards a new mapping of brain cortex function. Cerebrovascular diseases. 2004; 17(Suppl 3):35. [PubMed: 14730257]
56. Vanzetta I, Grinvald A. Increased cortical oxidative metabolism due to sensory stimulation: implications for functional brain imaging. Science. 1999; 286:1555–1558. [PubMed: 10567261]
57. Tomasi D, Wang GJ, Volkow ND. Energetic cost of brain functional connectivity. Proceedings of the National Academy of Sciences of the United States of America. 2013; 110:13642–13647. [PubMed: 23898179]
58. Madisen L, et al. A robust and high-throughput Cre reporting and characterization system for the whole mouse brain. Nature neuroscience. 2010; 13:133–140. [PubMed: 20023653]
59. Acharya A, et al. The bHLH transcription factor Tcf21 is required for lineage-specific EMT of cardiac fibroblast progenitors. Development. 2012; 139:2139–2149. [PubMed: 22573622]
60. Diaz F, McKeehan N, Kang W, Hebert JM. Apoptosis of glutamatergic neurons fails to trigger a neurogenic response in the adult neocortex. The Journal of neuroscience : the official journal of the Society for Neuroscience. 2013; 33:6278–6284. [PubMed: 23575827]
61. Regan MR, et al. Variations in promoter activity reveal a differential expression and physiology of glutamate transporters by glia in the developing and mature CNS. The Journal of neuroscience : the official journal of the Society for Neuroscience. 2007; 27:6607–6619. [PubMed: 17581948]
62. Lovatt D, et al. The transcriptome and metabolic gene signature of protoplasmic astrocytes in the adult murine cortex. The Journal of neuroscience : the official journal of the Society for Neuroscience. 2007; 27:12255–12266. [PubMed: 17989291]
63. Cahoy JD, et al. A transcriptome database for astrocytes, neurons, and oligodendrocytes: a new resource for understanding brain development and function. The Journal of neuroscience : the official journal of the Society for Neuroscience. 2008; 28:264–278. [PubMed: 18171944]
64. Wang F, et al. Astrocytes modulate neural network activity by Ca(2)+-dependent uptake of extracellular K+ Science signaling. 2012; 5:ra26. [PubMed: 22472648]
65. Cidad P, Garcia-Nogales P, Almeida A, Bolanos JP. Expression of glucose transporter GLUT3 by endotoxin in cultured rat astrocytes: the role of nitric oxide. Journal of neurochemistry. 2001; 79:17–24. [PubMed: 11595753]
66. Hara M, Matsuda Y, Hirai K, Okumura N, Nakagawa H. Characteristics of glucose transport in neuronal cells and astrocytes from rat brain in primary culture. Journal of neurochemistry. 1989; 52:902–908. [PubMed: 2537381]
67. Rangroo Thrane V, et al. Ammonia triggers neuronal disinhibition and seizures by impairing astrocyte potassium buffering. Nature medicine. 2013; 19:1643–1648.
68. Wang X, et al. Astrocytic Ca2+ signaling evoked by sensory stimulation in vivo. Nature neuroscience. 2006; 9:816–823. [PubMed: 16699507]
69. Deane R, Segal MB. The transport of sugars across the perfused choroid plexus of the sheep. The Journal of physiology. 1985; 362:245–260. [PubMed: 4020688]

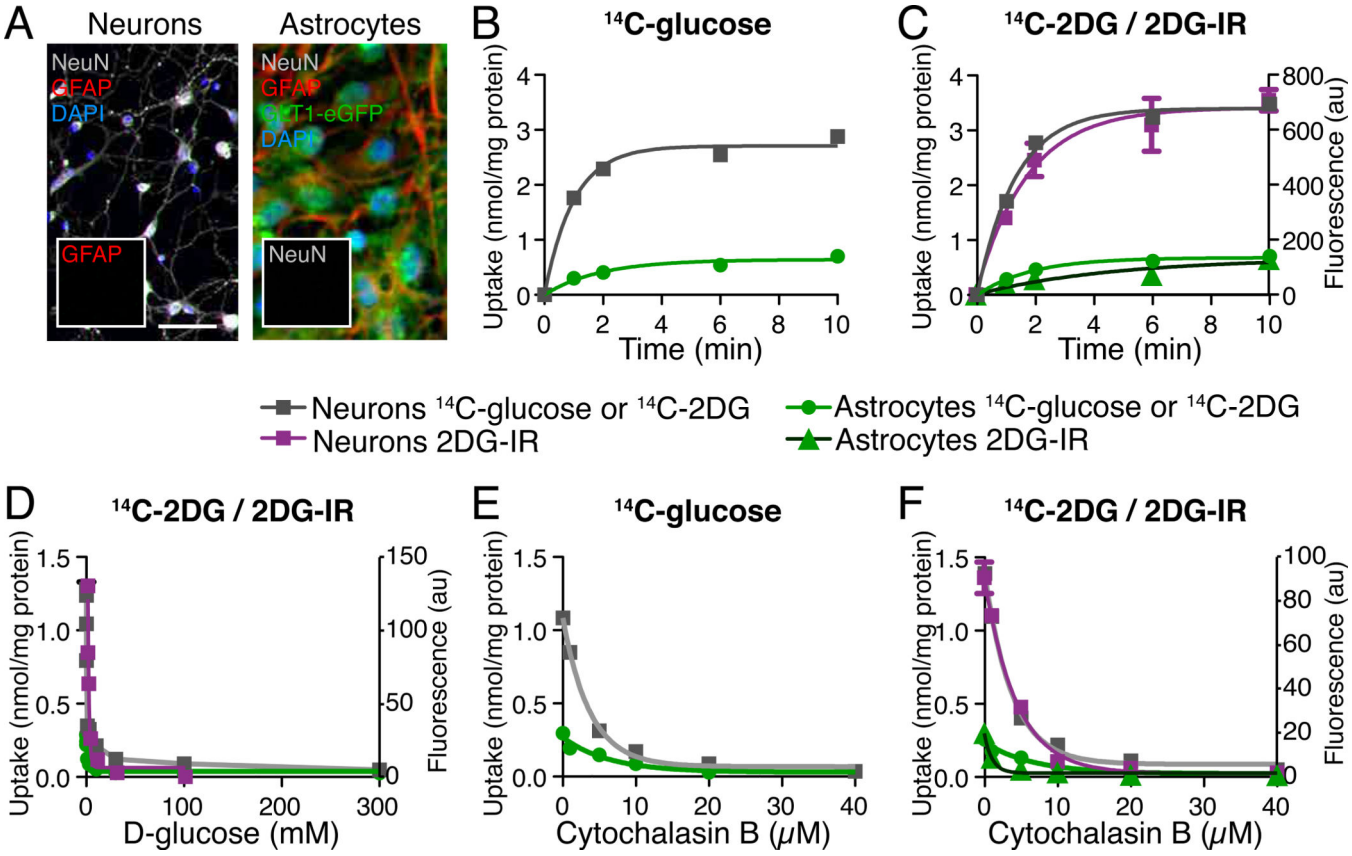

Figure 1. Preferential neuronal uptake of glucose and glucose analogues *in vitro*

(**A**) Immunocytochemistry of NeuN (grey), GFAP (red) and DAPI (blue) in neuronal cultures from wild type mice (left) and astrocyte cultures from GLT1-eGFP mice (right). Insert: GFAP (left) and NeuN (right) staining signals alone showed no staining signals. Scale bar, 50 μm. (**B**) ^{14}C-glucose uptake and (**C**) ^{14}C-2DG and 2DG-IR uptake in neurons and astrocytes plotted as a function of time. Slopes for initial linear phase ^{14}C-glucose neurons, 1.15 ± 0.06; ^{14}C-glucose astrocytes, 0.20 ± 0.01; ^{14}C-2DG neurons, 1.39 ± 0.03; ^{14}C-2DG astrocytes, 0.23 ±0.01 (nmol/mg protein/min); 2DG-IR neurons, 245.00 ± 30.52; 2DG-IR astrocytes, 28.17 ± 1.41 (in arbitrary units, au/min). (**D**) Substrate competition of ^{14}C-2DG and 2DG-IR uptake plotted as a function of increasing concentration of D-glucose (Ki in mM: ^{14}C-2DG neurons, 0.41 ± 0.01, 2DG-IR neurons, 0.87 ± 0.04, ^{14}C-2DG astrocytes, 0.71 ± 0.0 (**E**) Effect of increasing concentrations of the nonspecific glucose transporter inhibitor, cytochalasin B, on ^{14}C-glucose uptake (Ki in μM: ^{14}C-glucose neurons, 2.58 ± 0.11, ^{14}C-glucose astrocytes, 4.39 ± 0.03). (**F**) The effect of cytochalasin B effect on ^{14}C-2DG and 2DG-IR uptake (Ki in μM: ^{14}C-2DG neurons, 2.59 ± 0.04, 2DG-IR neurons, 3.02 ± 0.23; ^{14}C-2DG astrocytes, 4.64 ± 0.06; 2DG-IR astrocytes, 1.66 ± 0.06). The cultures were pretreated with cytochalasin B for 10 min prior to addition of ^{14}C-glucose, ^{14}C-2DG, or 2DG-IR. All values are expressed as mean ± s.e.m.

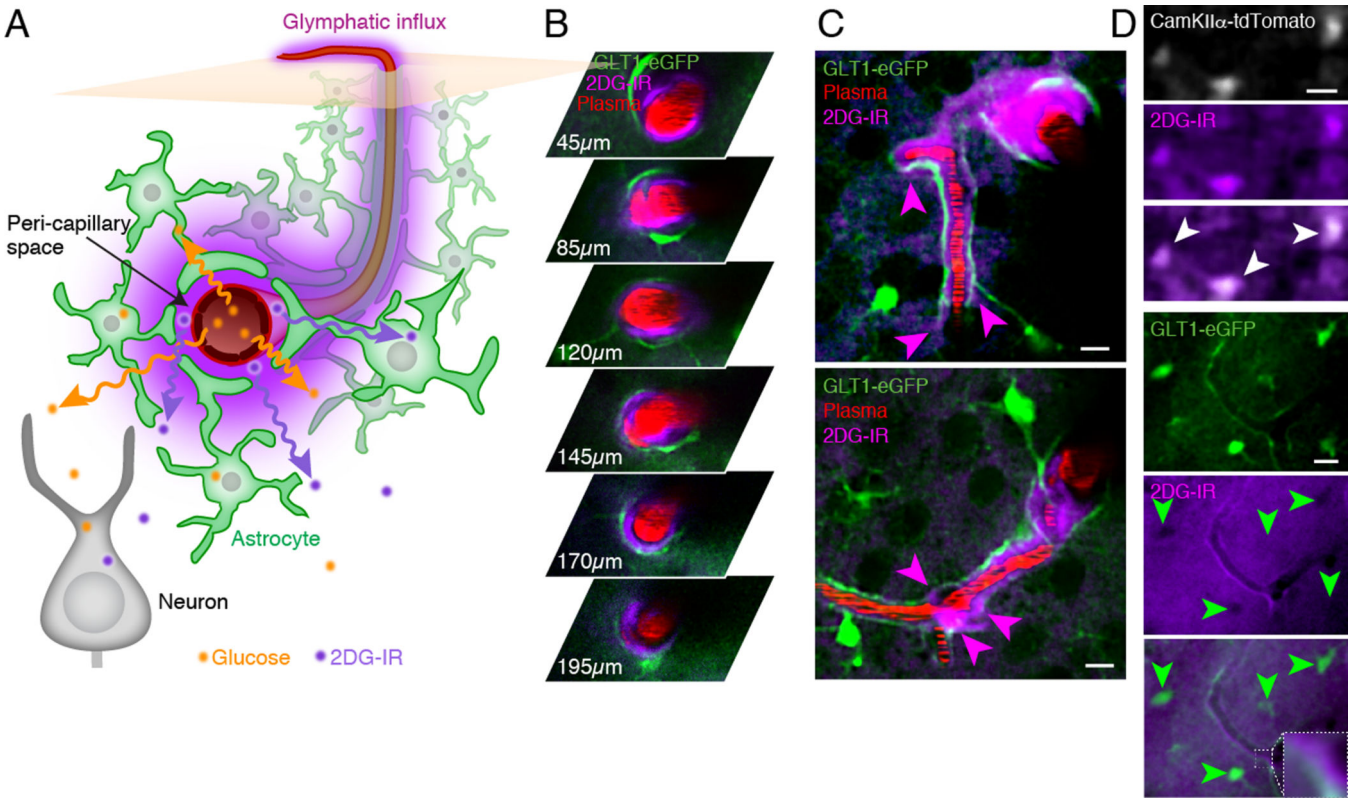

Figure 2. ***In vivo*** **imaging of cellular uptake of a near-infrared glucose analogue, 2DG-IR**

(**A**) Diagram illustrating the entry route of 2DG-IR via the peri-arterial space. 2DG-IR can be delivered either to the CSF via injection in cisterna magna or via micro-injection in the peri-arterial space surrounding cortical penetrating arteries. The CSF influx pathway is similar to vascular delivery of glucose, since glucose must, after crossing the blood brain barrier (BBB), pass the peri-vascular space prior to gaining access to neurons and astrocytes. (**B**) Representative high magnification *in vivo* images at serial depths of 2DG-IR in peri-arterial space surrounding penetrating arteriole at 5 min after injection (N=8). (**C**) 2DG-IR is transported along the peri-vascular space around both arteries and capillaries followed by diffusion into the tissue 5 min after injection (white arrows) (N=8). (**D**) *Upper panels* 2DG-IR uptake in a CamKII-EGFP neuronal reporter mouse showing that the highest 2DG-IR signal co-localizes with CamKII-EGFP^{+} neuronal cells bodies (white arrows) (N=3). *Lower panels* In contrast, 2DG-IR uptake in GLT1-EGFP^{+} astrocytes (green arrows) is either lower or comparable to surrounding neuropil (N=8). *Insert* Higher magnification of the capillary wall showing that the high 2DG-IR signal is localized in the peri-capillary space and surrounded by EGFP^{+} vascular endfeet of astrocytes. Scale bars, 10 μm in **C–D**.

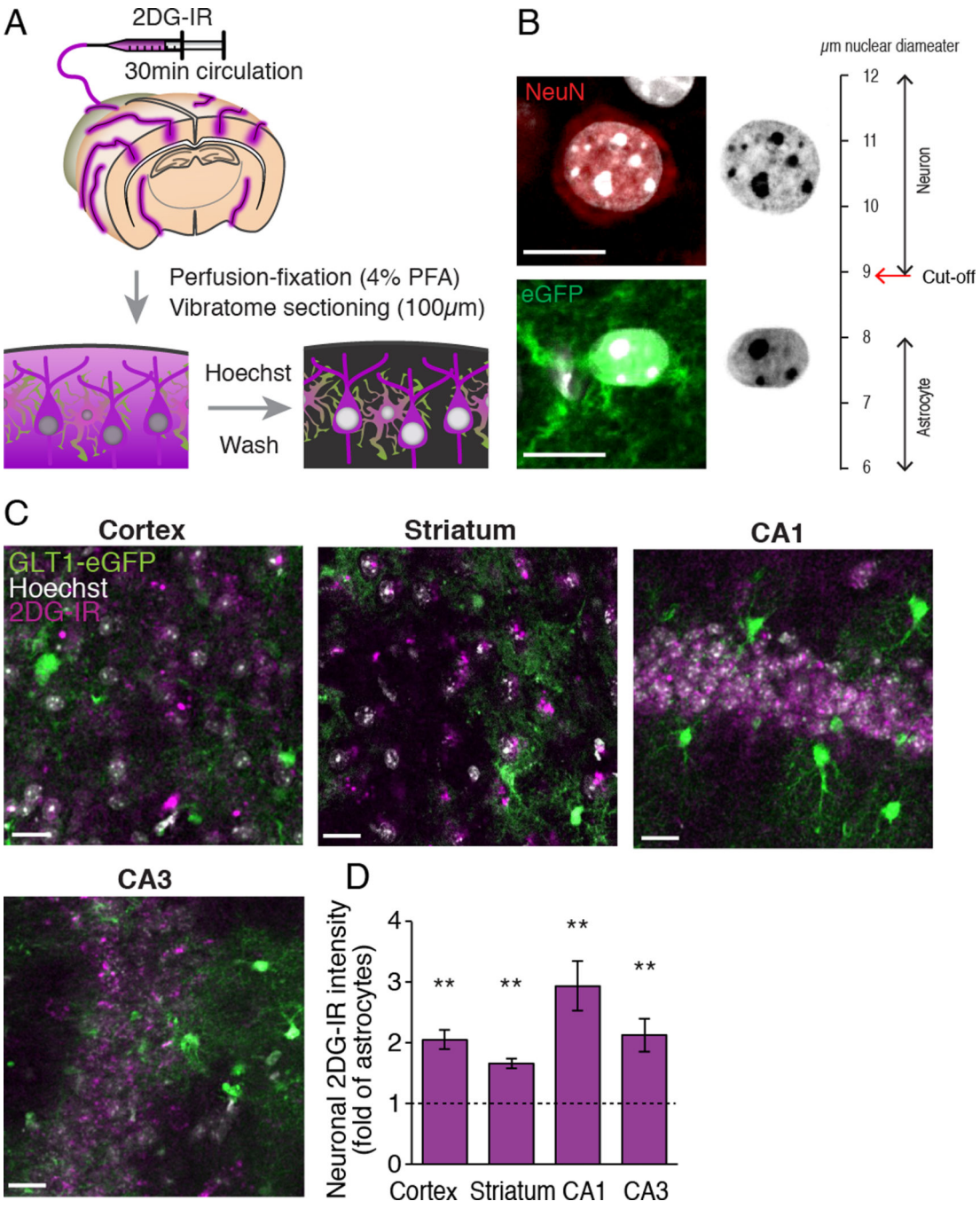

Figure 3. Quantitative comparison of neuronal and astrocytic uptake of 2DG-IR

(**A**) Diagram illustrating entry of 2DG-IR into the brain via peri-arterial routes following CSF injection in GFAP-eGFP reporter mice. After 30 min circulation of 2DG-IR, the animals are perfusion-fixed with 4% paraformaldehyde and 100 μm thick vibratome sections prepared. Before imaging, the slices are washed repeatedly to remove the glucose analogue not trapped in the cytosol and the nuclei were stained with yellow-Hoechst. (**B**) Neurons were identified in the freshly prepared vibratome sections by their large round nuclei and absence of cytosolic eGFP (10.2 ± 0.7 μm diameter). Astrocytes were recognized by their

smaller nuclei and eGFP signal (7.1 ± 0.1 μm diameter, P=0.01, t-test. N=3 mice). Scale bars, 10 μm. (**C**) Representative images of 2DG-IR uptake by neurons and astrocytes in cortex, striatum, CA1 and CA3 in awake GLT1-eGFP mice. Nuclei were stained with yellow-Hoechst (white). Scale bars, 20 μm. (**D**) Quantification of the ratio of 2DG-IR uptake in neurons vs astrocytes. P<0.001 in cortex and striatum, p=0.002 in CA1, P=0.006 in CA3, paired t test, neurons compared to astrocytes (N=9, 6, 8, 7 for cortex, striatum, CA1 and CA3, respectively). Bar graphs represent mean ± s.e.m.

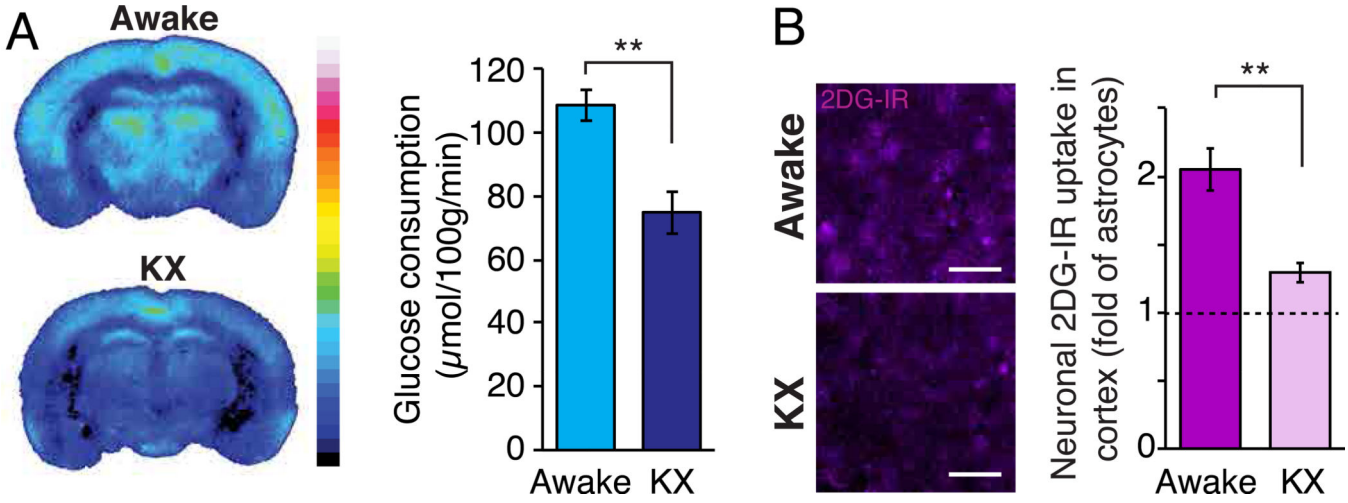

Figure 4. Anesthesia preferentially reduces neuronal 2DG-IR uptake

(**A**) **Left**: Representative ^{14}C-2DG autoradiographs of awake and anesthetized mice. **Right**: Quantifications of glucose consumption based on ^{14}C-2DG autoradiography in cortex of awake and ketamine/xylazine anesthetized mice. P=0.001, t-test (N=5). (**B**) **Left**: Imaging of 2DG-IR in cortex of awake and mice anesthetized with ketamine, 100 mg/kg and xylazine, 10 mg/kg, i.p (KX). Scale bars, 20 μm. **Right**: Anesthesia reduced the ratio of neuronal vs. astrocytic 2DG-IR uptake in cortex. P=0.002, Mann-Whitney test, N=9 awake, N=6, anesthetized. Bar graphs represent mean ± s.e.m.

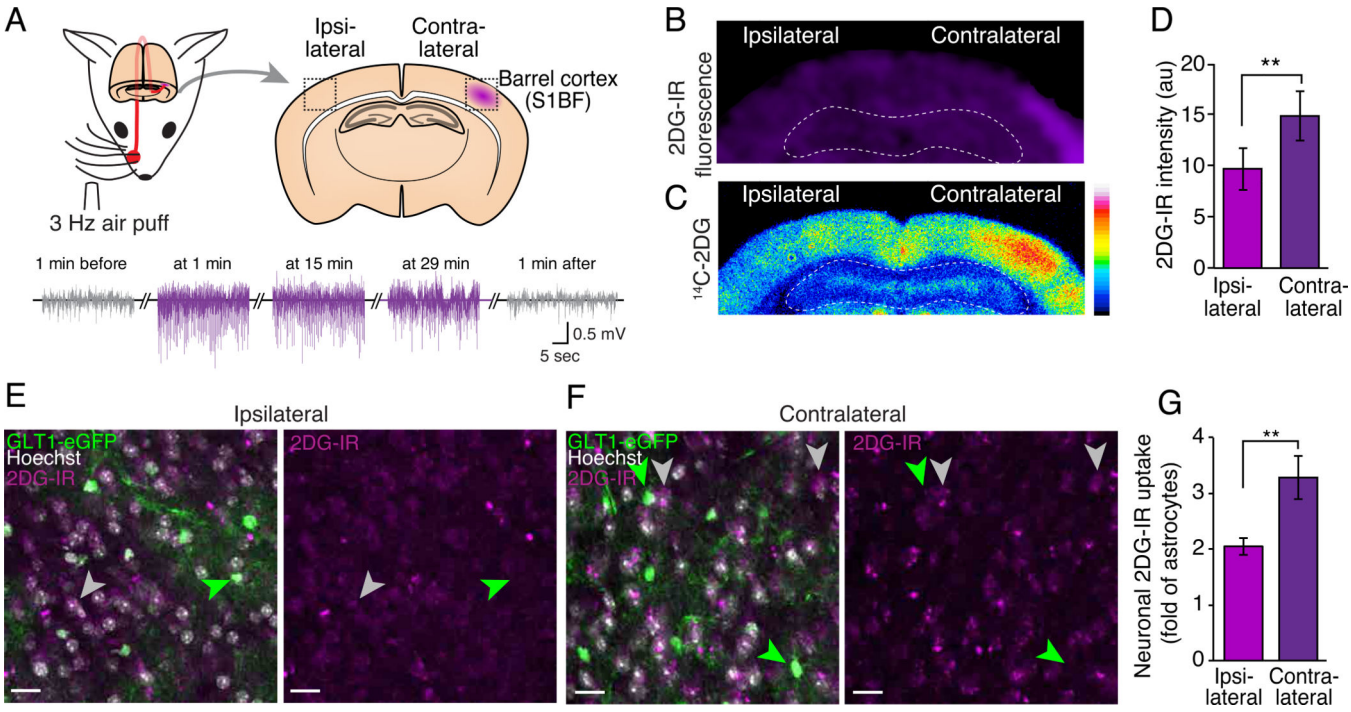

Figure 5. Functional activation increases neuronal uptake, but not astrocytic uptake of 2DG-IR

(**A**) **Upper panel**: Diagram of experimental setup. Whisker stimulation (air puffs, 3Hz, 30 min) induced an increase in uptake of 2DG-IR and ^{14}C-2DG in contralateral somatosensory barrel cortex (S1BF). **Lower panel**: Local field potential (LFP) recording in contralateral cortex 1 min before, 1, 15 and 29 min into the stimulation and 1 min after whisker stimulation. (**B**) Representative images of 2DG-IR fluorescence and (**C**) ^{14}C-2DG autoradiography of whisker stimulated mice. White dotted lines outline hippocampus. Contralateral cortex was 19 ± 4% higher than ipsilateral cortex. P<0.01, paired t test (N=5). (**D**) Quantification of 2DG-IR fluorescence in contralateral and ipsilateral barrel cortex in mice with whisker stimulation. P=0.003, paired t-test (N=7). Representative images of 2DG-IR uptake in neurons and astrocytes in (**E**) ipsilateral and (**F**) contralateral cortex of whisker stimulated mice. Scale bars, 20 μm. **Right panel**: Close-up images of 2DGIR in neurons and astrocytes in ipsi- and contralateral cortex with and without eGFP and yellow-Hoechst signals. (**G**) Quantification of 2DG-IR fluorescence in neurons relative to astrocytes in the respective regions. P=0.006, t test (N=7 contralateral and N=9 ipsilateral). Bar graphs represent mean ± s.e.m.

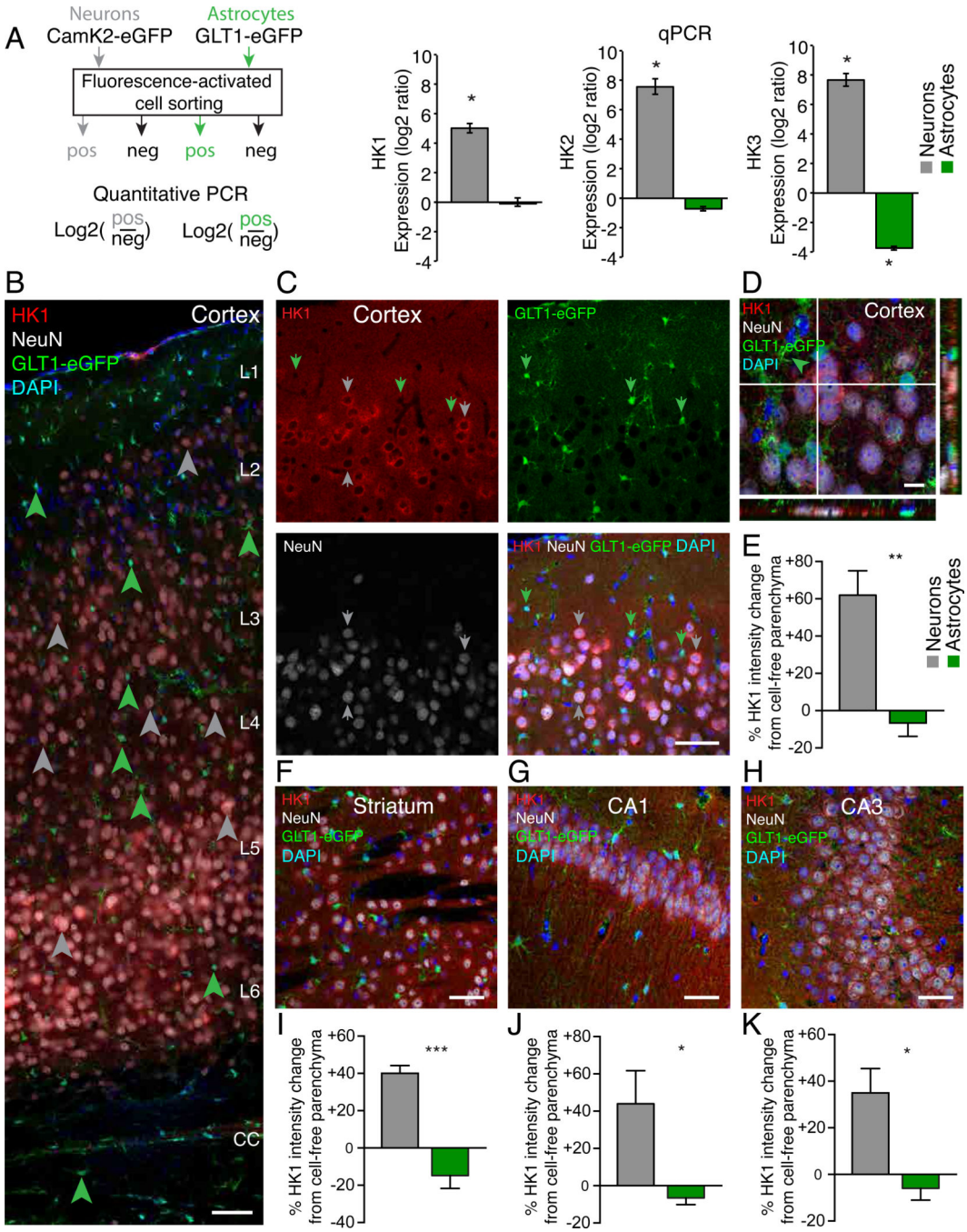

Figure 6. Neurons express high levels of hexokinases

(**A**) **Left:** Diagram of FACS sorting strategy for qPCR of HK1-3. **Right:** qPCR analysis of hexokinase (HK) 1–3 expression in FACS sorted cortical neurons (tdTomato^{+} vs tdTomato^{-} cell population harvested from Camk2a-CreERT2/CAG-tdTomato reporter mice) and astrocytes (eGFP^{+} vs eGFP^{-} cell populations harvested from GLT1-eGFP reporter mice) expressed as log2 of the ratio of positive vs negative population. P<0.05 compared to negative populations for HK1-3 in neurons and HK3 in astrocytes (N=3 mice in each group). (**B–C**) Immunohistochemistry of HK1 (red) in neurons (NeuN^{+}, grey arrow) and astrocytes

(green arrow, $eGFP^+$) with DAPI (blue) in cortex of a GLT1-eGFP reporter mouse. Scale bar, 50 μm. (**D**) Orthogonal projections of a 0.1 μm step size Z-stack. Green arrow indicates an astrocyte endfoot. (**E**) Quantification of HK1 immunoflourescence shown in percentage difference in HK1 immunolabeling intensity relative to cell-free parenchyma in the cytosol of $NeuN^+$ neurons (grey) and GLT1-$eGFP^+$ astrocytes (green) in cortex. $P<0.01$, t-test (40 neurons and 40 astrocytes from N=4 mice). (**F–H**) Immunohistochemistry of HK1 and NeuN in GLT1-eGFP mouse and (**I,J,K**) percentage difference in immunolabeling intensity relative to cell-free parenchyma in striatum, CA1 and CA3, respectively. Scale bars, 50 μm in **F–H**, $P<0.001$ for striatum, $P<0.05$ for CA1 and CA3, t test (40 neurons and 40 astrocytes in N=4 mice). Bar graphs represent mean ± s.e.m.

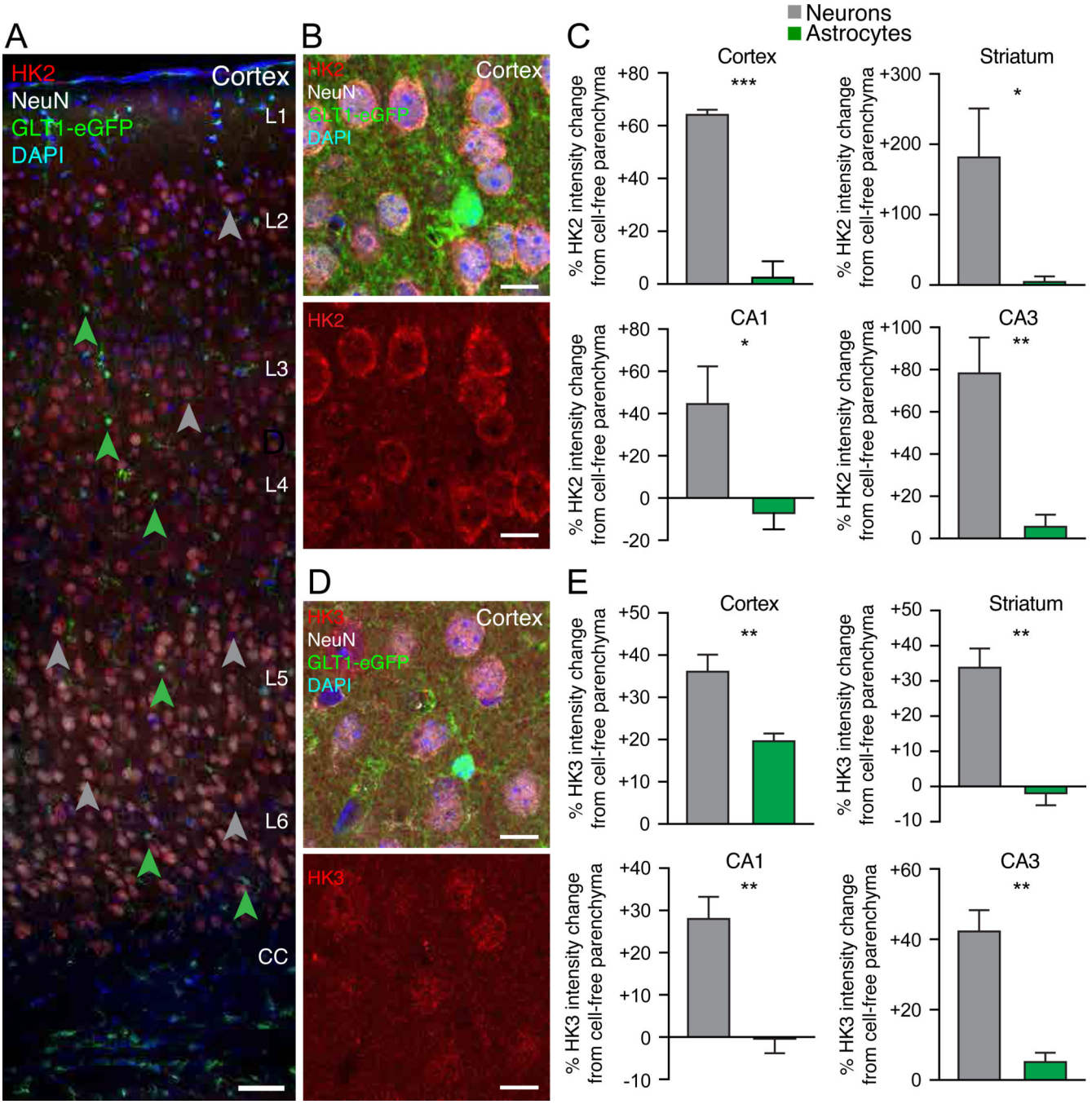

Figure 7. Neurons express high levels of hexokinase 2 and 3

(**A**) Immunohistochemistry of HK2 (red) in neurons (NeuN$^+$, grey arrow) and astrocytes (green arrow, eGFP$^+$) with DAPI (blue) of a GLT1-eGFP reporter mouse from the surface of cortex through to the corpus callosum. Scale bar, 50 μm. (**B**) HK2 (red) and NeuN (white) immunohistochemistry in GLT1-eGFP mouse cortex. Scale bar, 50 μm. (**C**) Percentage difference in HK2 immunolabeling intensity relative to cell-free parenchyma in the cytosol of NeuN$^+$ neurons (grey) and GLT1-eGFP$^+$ astrocytes (green) in cortex ($P<0.001$), striatum ($P<0.05$), CA1 ($P<0.05$) and CA3 ($P<0.01$), t test (30–50 neurons and 30–50 astrocytes in

N=4 mice). (**D**) HK3 (red) and NeuN (white) immunohistochemistry in GLT1-eGFP mouse cortex. Scale bar, 50 μm. (**E**) Percentage difference in HK3 immunolabeling intensity relative to cell-free parenchyma in the cytosol of $NeuN^+$ neurons (grey) and GLT1-$eGFP^+$ astrocytes (green) in cortex, striatum, CA1 and CA3. $P<0.01$, t test (35–50 neurons and 35–50 astrocytes in N=4 mice). Bar graphs represent mean ± s.e.m.

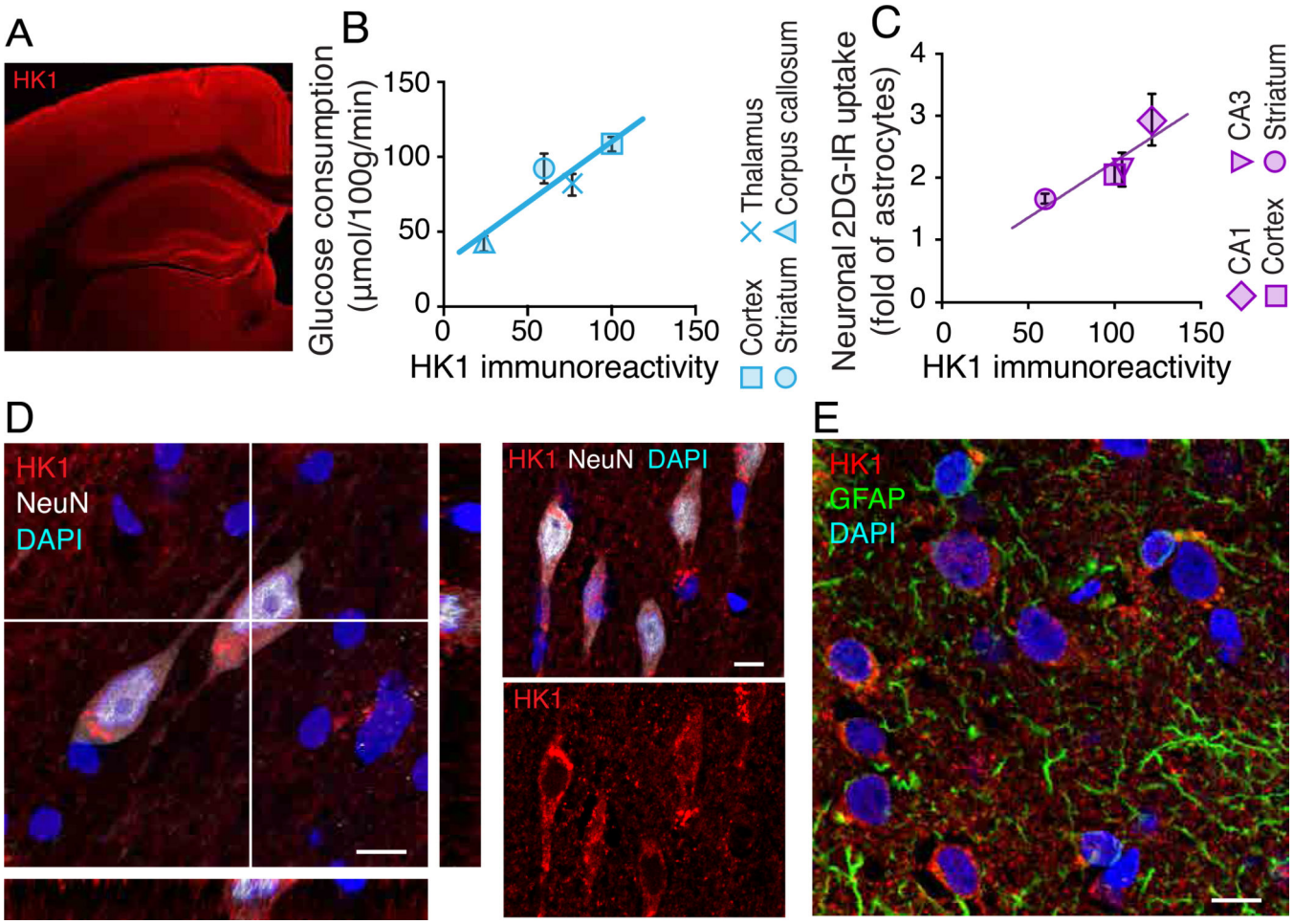

Figure 8. Correlation of hexokinase with glucose consumption and its expression in human brain

(**A**) Hexokinase 1 (HK1) immunohistochemistry of mouse brain. (**B**) Glucose consumption calculated from ^{14}C-2DG signal in cortex, striatum, thalamus, and corpus callosum plotted against HK1 immunoreactivity in the same area. Correlation coefficient R^2=0.85 (N=5 for HK1 quantification, N=5 for autoradiography). (**C**) The ratio of neuronal vs astrocytic 2DG-IR uptake plotted against HK1 immunoreactivity in cortex, striatum, hippocampal CA1 and CA3 regions. Correlation coefficient R^2=0.78 (N=5 for HK1 quantification, N=6–9 for 2DG-IR uptake). (**D**) Orthogonal projections of a 0.1 µm step size Z-stack and image of HK1 (red) and NeuN (grey) immunohistochemistry of adult human cortex. (**E**) Immunohistochemistry of HK1 (red) and GFAP (green) in adult human cortex. Scale bars in **D–E**, 10 µm.